Modulation of Marine Low Clouds Associated with the Tropical Intraseasonal Variability over the Eastern Pacific

XIANAN JIANG

Joint Institute for Regional Earth System Science & Engineering, University of California, Los Angeles, and Jet Propulsion Laboratory, California Institute of Technology, Pasadena, California

TERENCE L. KUBAR

Jet Propulsion Laboratory, California Institute of Technology, Pasadena, California, and Colorado State University, Fort Collins, Colorado

SUN WONG

Jet Propulsion Laboratory, California Institute of Technology, Pasadena, California

WILLIAM S. OLSON

Joint Center for Earth Systems Technology, University of Maryland, Baltimore County, Baltimore, Maryland

DUANE E. WALISER

Jet Propulsion Laboratory, California Institute of Technology, Pasadena, California

(Manuscript received 19 September 2013, in final form 31 March 2014)

ABSTRACT

Owing to its profound influences on global energy balance, accurate representation of low cloud variability in climate models is an urgent need for future climate projection. In the present study, marine low cloud variability on intraseasonal time scales is characterized, with a particular focus over the Pacific basin during boreal summer and its association with the dominant mode of tropical intraseasonal variability (TISV) over the eastern Pacific (EPAC) intertropical convergence zone (ITCZ). Analyses indicate that, when anomalous TISV convection is enhanced over the elongated EPAC ITCZ, reduction of low cloud fraction (LCF) is evident over a vast area of the central North Pacific. Subsequently, when the enhanced TISV convection migrates to the northern part of the EPAC warm pool, a "comma shaped" pattern of reduced LCF prevails over the subtropical North Pacific, along with a pronounced reduction of LCF present over the southeast Pacific (SEPAC). Further analyses indicate that surface latent heat fluxes and boundary heights induced by anomalous low-level circulation through temperature advection and changes of total wind speed, as well as midlevel vertical velocity associated with the EPAC TISV, could be the most prominent factors in regulating the intraseasonal variability of LCF over the North Pacific. For the SEPAC, temperature anomalies at the top of the boundary inversion layer between 850 and 800 hPa play a critical role in the local LCF intraseasonal variations. Results presented in this study provide not only improved understanding of variability of marine low clouds and the underlying physics, but also a prominent benchmark in constraining and evaluating the representation of low clouds in climate models.

1. Introduction

Nearly one-third of the global ocean surface is covered by low-topped clouds (Klein and Hartmann 1993; Kubar et al. 2011). These marine low clouds exert pronounced influences on the earth's surface energy balance. By effectively reflecting incoming solar shortwave (SW) radiation, while not strongly affecting the longwave (LW) radiation, these low clouds induce a strong net negative radiative effect (e.g., Stephens and Greenwald 1991; Hartmann et al. 1992). It is suggested that the global cooling effect due to a moderate increase of low cloud

Corresponding author address: Dr. Xianan Jiang, Jet Propulsion Laboratory, California Institute of Technology, MS 233-300, 4800 Oak Grove Drive, Pasadena, CA 91109.
E-mail: xianan@jifresse.ucla.edu

DOI: 10.1175/JCLI-D-13-00569.1

coverage could effectively offset the warming due to a doubling of CO_2 (e.g., Randall 1984; Slingo 1990; Wood 2012). As essential tools for climate projection, current general circulation models (GCMs), however, exhibit significant uncertainties in modeling these marine low clouds and associated feedback processes (e.g., Cess et al. 1990; Bony and Dufresne 2005). Therefore, comprehensive understanding of physical processes regulating low cloud properties based on observations, including their spatial extent, optical depth, and temporal variability, is essential and urgent to improve and constrain representation of low clouds in climate models. While great achievements have been made in recent decades toward this effort, our understanding of factors controlling key low cloud properties remains limited.

Climatologically, marine low clouds largely reside over subtropical regions where large-scale subsidence prevails over a cool ocean surface (e.g., see Fig. 1a for boreal summer mean low cloud coverage and sea level pressure over the Pacific basin). Meanwhile, low clouds exhibit strong variability on a broad range of temporal and spatial scales. Variability of low clouds on interannual, seasonal, and synoptic time scales, and plausible processes responsible for this variability, have been previously investigated (e.g., Klein and Hartmann 1993; Klein et al. 1995; Rozendaal et al. 1995; Klein 1997; Norris and Klein 2000; Wood and Bretherton 2006; Stevens et al. 2007; Kubar et al. 2012; and many others). While no exclusive factors have been identified in regulating low cloud variability on all of these time scales, it has been suggested that lower-tropospheric stability tends to play an important role in modulating low cloud patterns on both interannual and annual cycle time scales (Klein and Hartmann 1993; Wood and Bretherton 2006). Additionally, cold-air advection and fluctuations of large-scale subsidence could be primarily responsible for synoptic variability of low clouds (Norris and Klein 2000). For a comprehensive review of previous studies on low cloud variability, the reader is referred to Wood (2012).

As to the variability of low clouds, while most of these aforementioned studies have focused on synoptic or seasonal-to-interannual time scales, rather limited attention has been placed on their subseasonal variability with a time scale of several weeks. It has been widely reported that tropical deep convection exhibits vigorous subseasonal fluctuations, generally referred to as tropical intraseasonal variability (TISV); see Lau and Waliser (2012) for a comprehensive review. While the strongest convective activity associated with the TISV is confined to the deep tropics, profound impacts of the TISV are detected over vast extratropics and mid to high latitudes through relaxation and enhancement of the Walker circulation and/or excitation of Rossby wave trains by diabatic

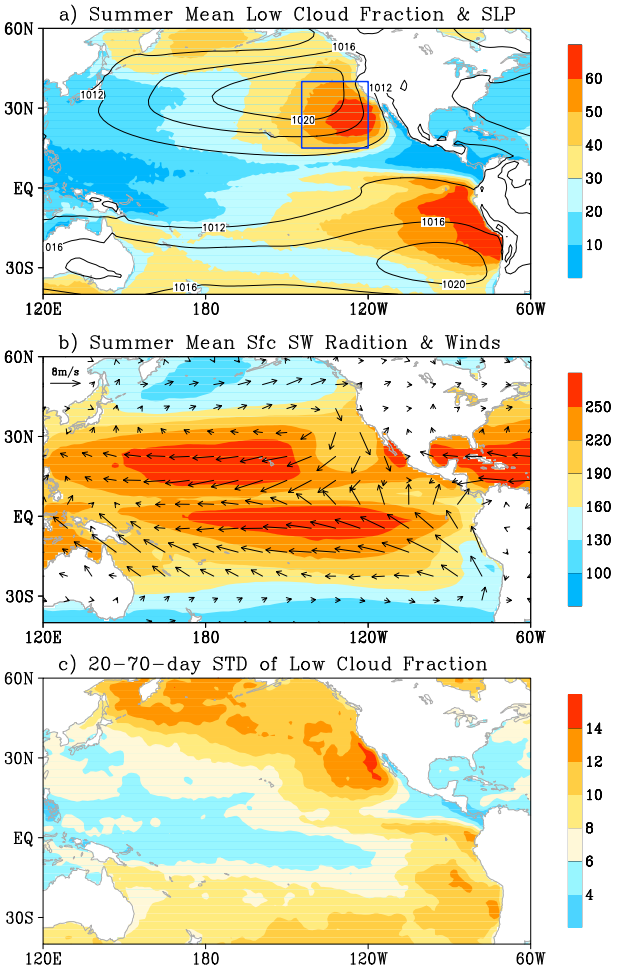

FIG. 1. Summer mean (May–October) (a) fraction of low cloud cover (%) based on the MODIS dataset (shaded) and sea level pressure (hPa, contours) and (b) downward net shortwave radiation (W m^{-2}) based on ISCCP (shaded) along with 10-m winds (see vector scale upper left of the panel). (c) Standard deviation (%) of 20–70-day bandpass-filtered low cloud fraction for May–October.

heating associated with the TISV convection (e.g., Knutson and Weickmann 1987; Ferranti et al. 1990; Higgins and Mo 1997; Jiang and Lau 2008). To the best of our knowledge, there have not been detailed reports on impacts of the TISV on marine low clouds, which is the main motivation of this study.

In this study, we will examine the variability of marine low clouds associated with the TISV over the eastern Pacific (EPAC) intertropical convergence zone (ITCZ), with a particular focus on the Pacific basin during boreal summer season. It has been reported that the maximum marine low cloud coverage over the Pacific Ocean occurs over the eastern part of the basin during boreal summer on both northern and southern sides of the EPAC ITCZ and warm pool regions, with one center near the coastal region off California and another near

the South American coast off the Andes (Fig. 1a; also see Kubar et al. 2012). Meanwhile, the TISV associated with the EPAC ITCZ exhibits its strongest amplitude during boreal summer (e.g., Maloney et al. 2008; Jiang and Waliser 2008, 2009). Thus, it is of interest to see how the intraseasonal variability in convective activity associated with the EPAC ITCZ can influence low cloud variability. In light of the quasiperiodic occurrence of the TISV, the plausible predictability of the TISV with lead times on the order of a couple of weeks could provide subseasonal predictability for marine low clouds (Neena et al. 2014, manuscript submitted *J. Climate*).

The outline of this paper is as follows. In section 2, datasets used for this study and the approach to identify marine low clouds are briefly described. In section 3, anomalous low cloud fraction patterns during different EPAC TISV phases will be illustrated. Possible large-scale factors responsible for the intraseasonal variability of low clouds over the Pacific basin will also be explored. A summary and discussion are presented in section 4.

2. Datasets and approaches

The primary observational dataset used for this study is the Moderate Resolution Imaging Spectroradiometer (MODIS) level-3 gridded daily product (Hubanks et al. 2008) for the period from September 2002 to August 2011. Daily mean cloud-top temperature and pressure, as well as histograms of pixel counts binned on 11 vertical levels for cloud-top pressure on each $1° \times 1°$ grid based on MODIS aboard *Aqua*, are used for this study. Daily mean cloud-top height on each grid is further derived by using the NOAA Optimum Interpolation Sea Surface Temperature (OISST) (Reynolds et al. 2007) and MODIS cloud-top temperature with a mean boundary layer lapse rate of $0.0069\,\mathrm{K\,m^{-1}}$ following Zuidema et al. (2009) and Kubar et al. (2012).

Low cloud grids are then identified largely following an approach described in Kubar et al. (2012) with slight modifications. For a grid point to be categorized as a low cloud, either of the following two conditions must be met: 1) daily mean cloud-top temperature is warmer than 270 K and cloud-top pressure greater than 500 hPa or 2) cloud-top temperature may be below 270 K, but cloud-top pressure must be greater than 500 hPa and cloud-top height must be less than 4 km. The second condition is mainly designed to capture those midlatitude low clouds that may be colder than 270 K. To restrict our analyses to those with relatively pure low cloud grids, cloud-top pressure for greater than 75% of total pixels within each low-cloud grid box must occur between one vertical layer above and below daily mean cloud-top pressure based on histograms of pixel counts along vertical levels. Once the cloud type on a grid is identified as low cloud, the fraction of cloudy pixels on this grid based on MODIS is then assigned as low cloud fraction.

Rainfall observations based on the Tropical Rainfall Measuring Mission (TRMM, version 3B42V6; Huffman et al. 1995) is employed to extract intraseasonal variability signals in convection over the EPAC ITCZ. The raw 3-hourly TRMM rainfall with a 0.25° spatial resolution was interpolated onto $1° \times 1°$ daily data. Following Jiang et al. (2012a), extended empirical orthogonal function (EEOF) analyses (Weare and Nasstrom 1982) of daily 20–70-day bandpass filtered rainfall anomalies over the EPAC (0°–30°N, 140°–90°W) from 1998 to 2012 are performed to define the leading tropical intraseasonal variability modes. The first two leading EEOF modes of daily rainfall anomalies capture the dominant TISV modes associated with the EPAC ITCZ (Jiang and Waliser 2008, 2009). These two leading principal components (PCs), which are in quadrature with each other, are used to determine daily TISV amplitudes and phases (ranging from 1 to 8, then back to phase 1) following a similar method employed in Wheeler and Hendon (2004) for the Madden–Julian oscillation (MJO). Note that the definition of each TISV phase applied here is based on a local TISV index over the EPAC; therefore it is independent from the MJO phase as defined by the Wheeler–Hendon index. Composite analyses for various variables including rainfall and low cloud fraction can then be conducted by averaging the bandpass-filtered anomalies of these variables over each TISV phase based on selected strong TISV events ($\sqrt{\mathrm{PC}_1^2 + \mathrm{PC}_2^2} \geq 1.0$) during the boreal summer season (May–October).

Daily meteorological fields including 3D winds, relative humidity, temperature, and surface pressure from the recent Interim European Centre for Medium-Range Weather Forecasts (ECMWF) Re-Analysis (ERA-Interim) (Dee et al. 2011) with a horizontal resolution of $1.5° \times 1.5°$, and net surface SW and LW radiation from the International Satellite Cloud Climatology Project (ISCCP) (Zhang et al. 2004) on 1° grids, are analyzed to explore physical factors regulating intraseasonal low cloud variability. In addition, daily 3D fields of TRMM-based estimate of latent heating by using a ''trained'' radiometer heating algorithm (Grecu et al. 2009) and radiative heating based on the Hydrologic Cycle and Earth's Radiation Budget (HERB) algorithm (L'Ecuyer and McGarragh 2010) are employed to examine vertical heating profiles in association with the intraseasonal low-cloud variability. These TRMM-based heating products have been used to characterize the vertical heating structure of the MJO (Jiang et al. 2009; Jiang et al. 2011). Except for the ISCCP surface radiation data, which only covers the period of 2002–09, all other variables from the same period of

MODIS data, that is, from September 2002 to August 2011, are analyzed in this study.

3. Results

a. *Climatology of low cloud over the Pacific Ocean during boreal summer*

Distribution of summer mean low cloud fraction (LCF) based on MODIS over the Pacific basin along with sea level pressure (SLP) is illustrated in Fig. 1a. Consistent with previous studies, maximum coverage of summer mean low clouds with a fraction exceeding 60% is observed on the eastern flanks of semipermanent subtropical highs in both hemispheres. Low cloud coverage with a fraction of 30%–40% is also evident over the North Pacific near 50°N and the subtropical region over the Southern Hemisphere. Along the Pacific ITCZ where northeasterly trade winds in the Northern Hemisphere meet with the southeasterly trade winds from the south (see vectors in Fig. 1b), and over the western and eastern Pacific warm pools, a minimum of mean LCF is evident due to the predominance of deep convective clouds.

Figure 1b also displays summer mean net surface downward SW radiation (shaded) based on ISCCP. The strongest downward SW radiation is seen on both sides of the Pacific ITCZ, largely indicating the dominance of large-scale downward motion over these regions. Particularly noteworthy is an area over the EPAC near the California coast, where considerably reduced surface SW radiation is noted compared to its surrounding areas. The shape of the reduced SW pattern largely mimics that of the local maximum LCF as shown in Fig. 1a, illustrating the significant role of low clouds in effectively reflecting the solar radiation. A minimum of mean SW radiation is also noted over the narrow coastal region over the southeastern Pacific off the Andes, again in agreement with the local maximum center in LCF in Fig. 1a.

Since variability of marine low clouds on intraseasonal time scales is the focus of the present study, the standard deviation (STD) of 20–70-day bandpassed filtered daily LCF during boreal summer is displayed in Fig. 1c. The strongest intraseasonal variability of LCF is found over the coastal region off California, in accordance with the local maximum mean LCF. A maximum LCF STD of about 14% is evident, which is about 20% of its summer mean value. In addition, relatively strong intraseasonal variability in LCF with a STD exceeding 8% is also evident over a widespread region of the Pacific Ocean basin.

b. *Intraseasonal variability of the EPAC ITCZ*

Figure 2 illustrates the evolution of composite anomalous rainfall (shaded) and surface winds (vectors) over the EPAC warm pool at different TISV phases defined in section 2. A typical life cycle of the TISV associated with the EPAC ITCZ as previously reported is readily seen in Fig. 2 (Maloney and Esbensen 2007; Jiang and Waliser 2008). An enhanced rainfall signal first emerges over the western part of the domain along 8°N at phase 1 (Fig. 2a). Subsequently, convection experiences rapid intensification, and meanwhile migrates eastward in the following phases. As the maximum convection center approaches the land area over Central America after phase 4 (Fig. 2d), while largely trapped along the coastal region off Central America, a northward migration of the TISV convection is clearly discerned. This eastward movement of the EPAC TISV along with a northward propagation component exhibits great resemblance to the leading TISV mode associated with the Asian summer monsoon. It was suggested that the easterly vertical shear of monsoonal circulation, which prevails over both the Indian/western Pacific and eastern Pacific warm pool regions during boreal summer, could play a critical role in regulating the northward propagation of the TISV convection (Jiang et al. 2004; Jiang and Waliser 2008).

Another important feature of the EPAC TISV is the association of southwesterly anomalous low-level winds corresponding to enhanced phases of the TISV convection over the EPAC (see Fig. 2 for TISV phases 4–6). Since the summer mean low-level wind is southwesterly over the EPAC warm pool, the enhanced surface latent heat flux due to the anomalous southwesterly ISV winds associated with positive TISV convection will facilitate a positive feedback for the growth of TISV disturbances. This wind–evaporation–convection feedback has been considered to be one of the essential processes responsible for local TISV instability (Maloney and Esbensen 2003). Modeling studies have also suggested that capturing realistic low-level mean winds over the EPAC warm pool in a GCM could be essential for good representation of the EPAC TISV in the model (Rydbeck et al. 2013; Jiang et al. 2013).

Previous studies suggested that the EPAC TISV could be a local expression of the globally circumnavigating MJO signals (Maloney and Esbensen 2003). In the observations, much of the EPAC TISV is indeed phase-locked to the MJO status over the western Pacific (Small et al. 2011; Rydbeck et al. 2013). Recent modeling studies, however, suggest that the EPAC TISV may also exist independently of the global MJO (Rydbeck et al. 2013; Jiang et al. 2012b, 2013). Further investigations are warranted for a complete understanding of the origin of the EPAC TISV.

In the next section, we will illustrate how the variability of LCF over the Pacific basin is associated with the TISV of the EPAC ITCZ.

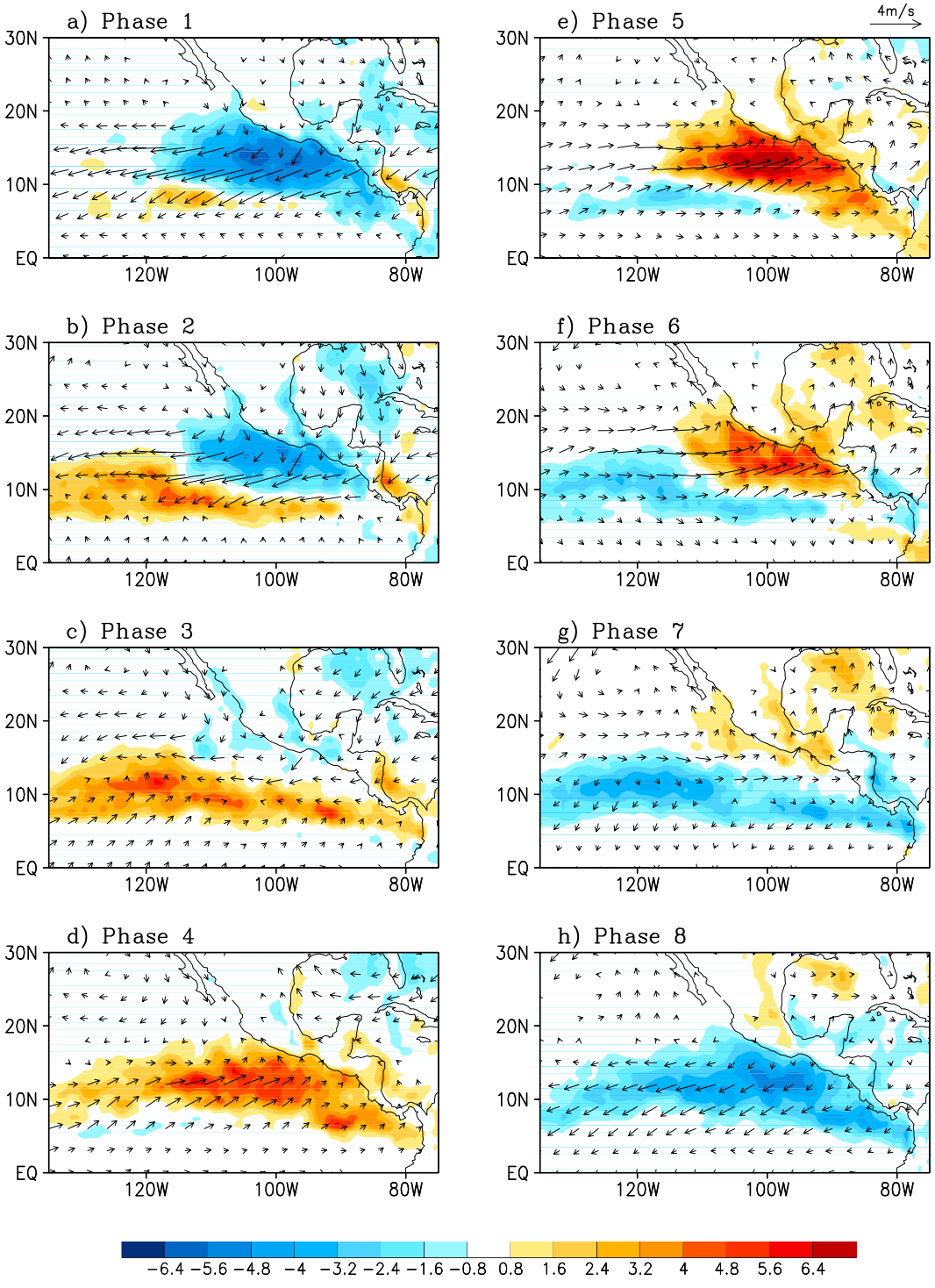

FIG. 2. Composite TRMM rainfall anomalies (mm day^{-1}) (shaded, see color scales at the bottom) at different EPAC TISV phases, along with corresponding anomalous 10-m winds (vectors, see upper right for vector scale).

c. *LCF variability associated with the TISV over the EPAC warm pool*

In Fig. 3, possible impacts of the EPAC TISV on LCF are examined by illustrating composite anomalous LCF (shaded) during different TISV phases, with regions where LCF anomalies surpass the 95% significance level stippled. Rainfall (pink contours) and 850-hPa wind (vectors) anomalies during the TISV evolution are also

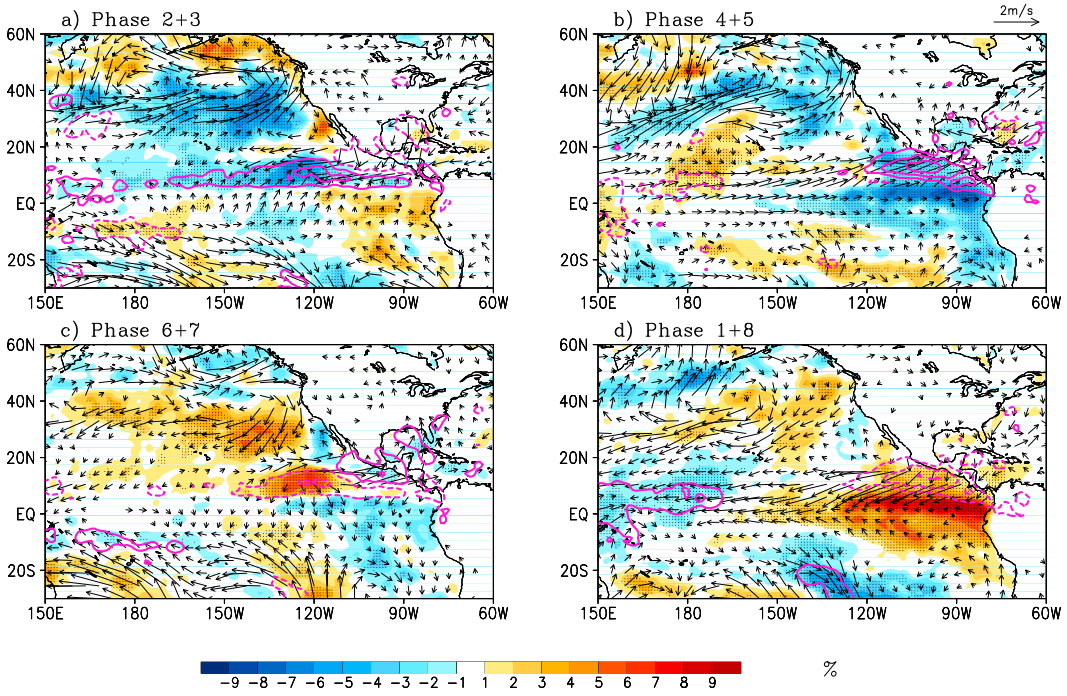

FIG. 3. Composite anomalous MODIS low-cloud fraction (shading, see scale bar at the bottom; regions with LCF anomalies surpassing 95% significance level are stippled), anomalous 10-m winds (vectors, based on ERA-Interim reanalysis), and TRMM rainfall [pink contours with solid (dashed) lines representing enhanced (suppressed) rainfall: first contour is ± 1 mm day^{-1}; interval 2 mm day^{-1} thereafter] during the evolution of the TISV over the eastern Pacific.

displayed, which were derived based on the exactly same approach as for Fig. 2 but with a greater spatial coverage. Also note that each composite plot displayed in Fig. 3 combines results during two consecutive TISV phases, namely, for TISV phases 2 + 3, 4 + 5, 6 + 7, and 1 + 8, respectively. Clearly evident in Fig. 3 is that LCF over the Pacific basin exhibits significant and organized variability associated with the EPAC TISV. During TISV phases 2 + 3 (Fig. 3a), when enhanced TISV convection is largely located over the elongated EPAC ITCZ, LCF is reduced over the vast region of the central North Pacific, while enhanced near the North American coast extending from California to the Aleutian Peninsula. Along with this LCF anomalous pattern, an anomalous low-level cyclonic circulation is present over the North Pacific. During the same period, LCF is also reduced over the EPAC ITCZ where the deep convection is enhanced. Weakly enhanced LCF is evident in the southeast Pacific (SEPAC) cold SST tongue region. During TISV phases 4 + 5 (Fig. 3b), as enhanced rainfall migrates to the northern part of the EPAC warm pool off the Mexican coast, anomalous 850-hPa cyclonic circulation over the North Pacific takes a slight northward expansion between 180° and 130°W; meanwhile, strong southwesterly anomalies are evident between 20° and 40°N, 150°E and 150°W. Reduced LCF over the North Pacific, which is characterized by a ''comma'' shape, tends to be closely collocated with cyclonic circulation and southwesterly anomalous winds. On the other hand, regions with enhanced LCF are noted to the west of the Hawaiian Islands and the North Pacific between 40° and 60°N, 150°E and 180°. Additionally, strong negative LCF anomalies are noticed over the SEPAC during TISV phases 4 + 5. Anomalous patterns of LCF and 850-hPa circulation during TISV phases 6 + 7 and phases 1 + 8 are largely opposite to those during phases 2 + 3 and 4 + 5, respectively.

It is worth noting that, while the maximum total intraseasonal variability in LCF is discerned over the coastal region off California as shown in Fig. 1c, the strongest LCF intraseasonal variability associated with the EPAC TISV in the Northern Hemisphere is evident over the central North Pacific, Gulf of Alaska, and the EPAC ITCZ in Fig. 3. This indicates that other systems in addition to the leading TISV mode over the EPAC as the focus of this analysis could play a role in modulating the intraseasonal variability of LCF near the California coast, such as the higher frequency intraseasonal variability modes previously described (Jiang and Lau 2008; Jiang and Waliser 2009; Wen et al. 2011).

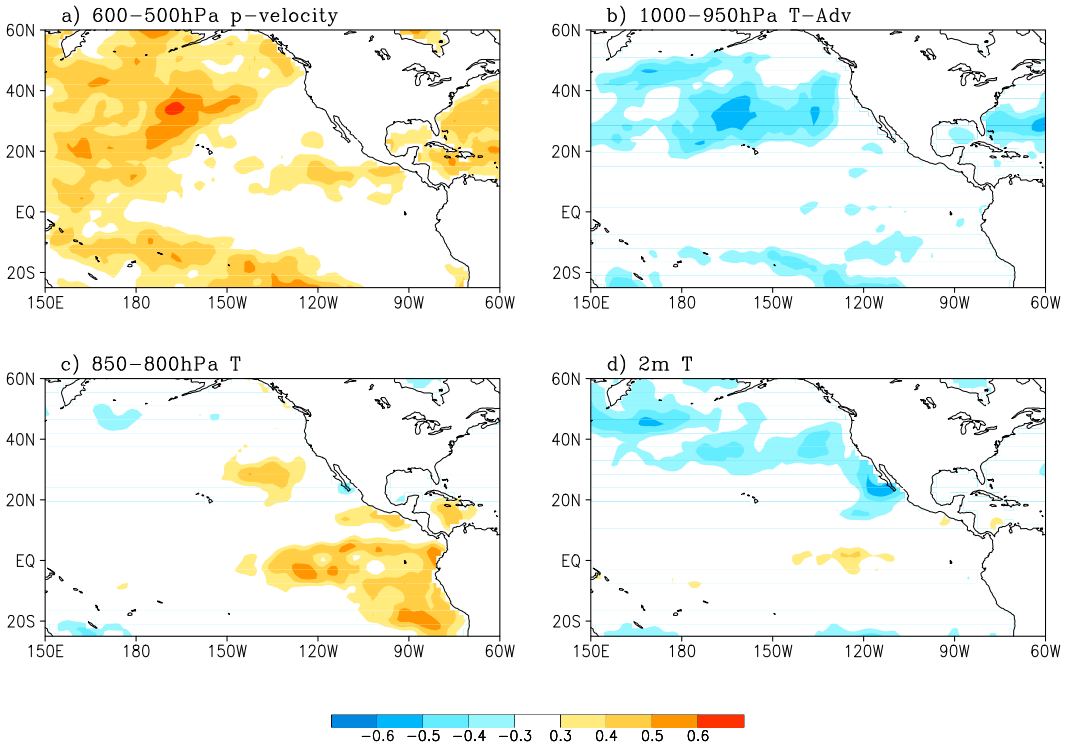

FIG. 4. Intraseasonal correlations for May–October from 2002 to 2011 between daily low-cloud fraction and (a) 600–500-hPa p vertical velocity, (b) 1000–950-hPa horizontal temperature advection, (c) 850–800-hPa temperature, and (d) 2-m temperature. Before calculating correlation coefficients on each grid point, all these above variables are subject to 20–70-day bandpass filtering. Only contours with absolute values of correlation coefficients greater than 0.3 are plotted, which roughly correspond to a 95% significance level based on a Student's t test.

To understand the key factors responsible for the intraseasonal variability of LCF during different TISV phases, correlations between LCF and various large-scale variables based on ERA-Interim reanalysis on each grid point are extensively explored for summer seasons from 2002 to 2011. These meteorological variables include 3D temperature (T), vertical velocity, horizontal T advection, SST, and 2-m T, as well as lower tropospheric stability (LTS), which is defined by the difference in potential temperature between 700 and 1000 hPa, following Klein and Hartmann (1993). It has been previously suggested that many of these above variables could be important in modulating LCF variability on various time scales. Since LCF variability on intraseasonal time scales is the focus of this study, both LCF and other variables are subject to a 20–70-day bandpass filtering before calculating temporal correlations. Analysis suggests that four variables—midlevel vertical velocity, low-level temperature advection, 850–800-hPa temperature, and 2-m temperature—could be most relevant in modulating the intraseasonal variability of LCF over different regions of the Pacific basin. Correlation patterns between local LCF and these four variables are illustrated in Fig. 4, where only contours with absolute values of correlation coefficients greater than 0.3 are plotted, which roughly corresponds to a 95% significance level based on a Student's t test.

Significant correlations between midlevel vertical motion and LCF on intraseasonal time scales are evident over large areas of the Pacific Ocean (Fig. 4a). Enhanced local LCF generally corresponds to anomalous downward motion in the midtroposphere. Maximum correlations are found over a region northwest of the Hawaiian Islands, with coefficients greater than 0.6. Over the SEPAC cold tongue region and in the region near the Californian coast, no significant correlations are noted between LCF and midlevel vertical motion. This correlation pattern between LCF and midlevel vertical motion on intraseasonal time scales is generally consistent with those derived for synoptic and seasonal time scales, as previously reported (Kubar et al. 2012). Increased inversion strength due to warming and drying associated with enhanced midlevel downwelling is largely responsible for the increase of low clouds. It is noteworthy that, over particular regions where mean midlevel downward motion is strong, such as the southeastern

North Pacific and SEPAC cold tongue region, intraseasonal variations in midlevel vertical velocity will not strongly disturb the mean vertical motion and, thus, may not lead to marked LCF changes. This may explain weak correlations between midlevel vertical velocity and LCF over these above, as shown in Fig. 4a.

Strong negative correlations between LCF and low-level (1000–925 hPa) horizontal T advection are also detected over the North Pacific with a minimum correlation of about −0.5 (Fig. 4b). This suggests LCF variability associated with the strengthening and weakening of the subtropical high and with changes in its position (Wood 2012), as shown by the anomalous circulation during different TISV phases in Fig. 3. Association between enhanced LCF and cold low-level temperature advection has also been reported for LCF variability on synoptic and monthly scales (Bretherton et al. 1995; Klein 1997; Kubar et al. 2012). It is generally considered that low-level cold T advection tends to increase upward surface heat fluxes, thus warming and moistening the planetary boundary layer (PBL) from below; meanwhile, it reduces SST and increases static stability through associated enhanced surface wind, thus leading to an increase of LCF (Ronca and Battisti 1997; Klein 1997). Significant negative correlations between LCF and T advection are also detected over spotty areas in the Southern Hemisphere.

While relatively weak and insignificant correlations between LCF and temperature fields are noted over the North Pacific, significant correlations between LCF and 850–800-hPa temperatures are discerned over the SEPAC (Fig. 4c). Physics associated with enhanced LCF and warm 850–800-hPa temperature over this region will be discussed further below. Additionally, significant negative correlations between 2-m T and LCF are noted over part of the North Pacific (Fig. 4d) and are largely collocated with cold low-level T advection (Fig. 4b). It is worth noting that, while LTS has been found to be associated with LCF variability on various time scales over the Pacific basin (Klein and Hartmann 1993), significant correlations between LCF and LTS are only detected in very limited and spotty regions (not shown). Correlations are not significantly improved if, instead, the estimated inversion strength (Wood and Bretherton 2006) is used to represent the low-level stability.

To further examine how large-scale conditions associated with the EPAC ISV modulate LCF over the Pacific basin, composite anomalous fields of 600–500-hPa vertical velocity, 1000–950-hPa horizontal T advection, and 2-m T during different TISV phases are displayed in Fig. 5. Since patterns during TISV phases 6 + 7 and 1 + 8 largely mirror those during phases 2 + 3 and 4 + 5, only anomalous patterns of these composite fields during TISV phases 2 + 3 and 4 + 5 are shown. Over tropical regions, anomalous midlevel vertical velocity patterns during both TISV phases are consistent with TISV convective activity. Upward motion along the EPAC ITCZ belt during TISV phases 2 + 3 corresponds well to enhanced convective activity (cf. Figs. 3a and 5a), whereas during TISV phase 4 + 5, in association with local enhanced convection, strong midlevel upward motion is mainly confined to the EPAC warm pool (Fig. 5b). Over the subtropical North Pacific, a belt of anomalous rising motion is observed along 40°N extending from 150°E to the North American west coast during TISV phase 2 + 3, consistent with the anomalous cyclonic circulation over the North Pacific (Fig. 3a). This upward motion may partially explain the reduced LCF in the central North Pacific during this TISV period, particularly for the western part of the North Pacific basin where stronger correlations between midlevel vertical velocity and LCF are noted (Fig. 4a and the hatched area in Fig. 5a). Moreover, anomalous downward motion over the Gulf of Alaska and to the south of Kamchatka Peninsula near 150°E may be responsible for local enhanced LCF during TISV phase 2 + 3. During TISV phase 4 + 5, anomalous downward motion is noted south of the Kamchatka Peninsula and over a small region northwest of the Hawaiian Islands (Fig. 5b), in agreement with the local enhanced LCF. Meanwhile, anomalous upward motion is largely present over the remaining area in the North Pacific, which is in general agreement with the comma-shaped reduced LCF over these regions, and suggests the role of midlevel upward motion in regulating the LCF over the North Pacific during TISV phase 4 + 5.

The composite 1000–950-hPa anomalous T-advection field during phase 2 + 3 largely exhibits warm advection anomalies over the subtropical North Pacific and cold anomalies to the south of the Kamchatka Peninsula between 40° and 60°N, 150°E and 180° (Fig. 5c). Spatial distribution of warm and cold T advection is generally consistent with reduced and enhanced LCF over these two areas, respectively. During TISV phase 4 + 5, low-level T-advection anomalies are mainly characterized by warm and cold anomalies over the southeast and northwest parts in the subtropical North Pacific, and are closely associated with reduced and enhanced LCF over these two regions. Of particular interest is that the comma-shaped warm low-level T-advection pattern over the subtropical North Pacific that strongly resembles the reduced LCF pattern discussed in Fig. 3b, suggesting possibly important impacts of low-level T advection on LCF during this TISV phase. Warm (cold) temperature advection anomalies in Figs. 5c and 5d are largely in agreement with the southerly (northerly) anomalous

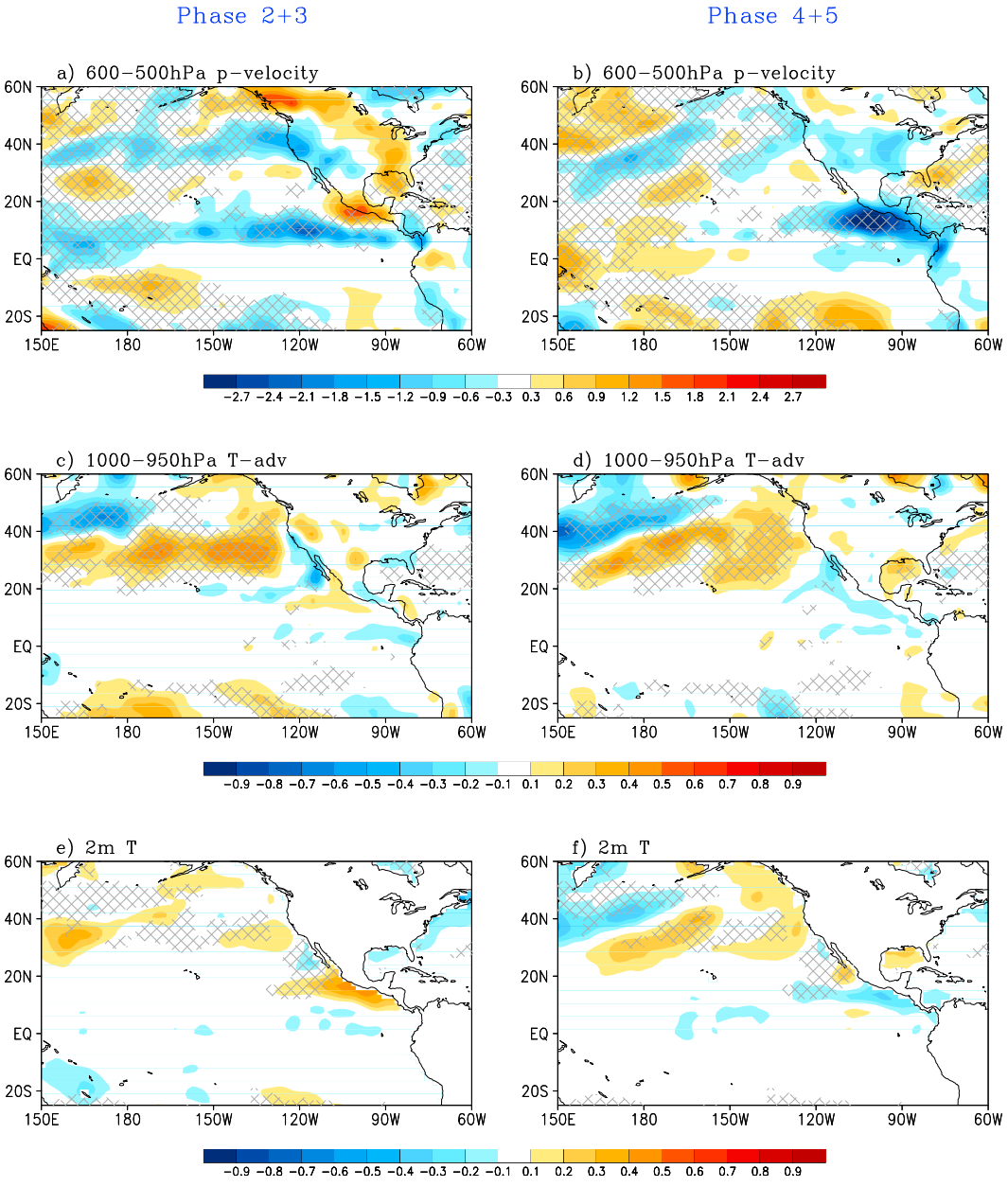

FIG. 5. Composite anomalous fields of (a),(b) 600–500-hPa p vertical velocity (10^{-2} Pa s^{-1}), (c),(d) 1000–950-hPa temperature advection (K day^{-1}), and (e),(f) 2-m temperature (K) during TISV phases (left) 2 + 3 and (right) 4 + 5. Grids are hatched in each panel where absolute values of correlation coefficients between the corresponding variable and local LCF exceed 0.3 as shown in Fig. 3.

wind component depicted in Figs. 3a and 3b, which suggests that advection of the mean low-level temperature by the anomalous circulation associated with the TISV is mainly responsible for the low-level T-advection patterns.

The correlation analysis above (Fig. 4d) indicates a negative relation between LCF and 2-m T in some small areas over the North Pacific. The composite 2-m T anomalous pattern during TISV phase 4 + 5, as shown in Fig. 5f, also suggests that cold and warm 2-m T anomalies near 40°N and south between 150°E and 150°W, respectively, could also contribute to enhanced and reduced LCF over these two regions. These cold and warm 2-m T anomalous patterns are also largely in agreement with the low-level T-advection pattern in Fig. 5d, although with a relatively weak amplitude.

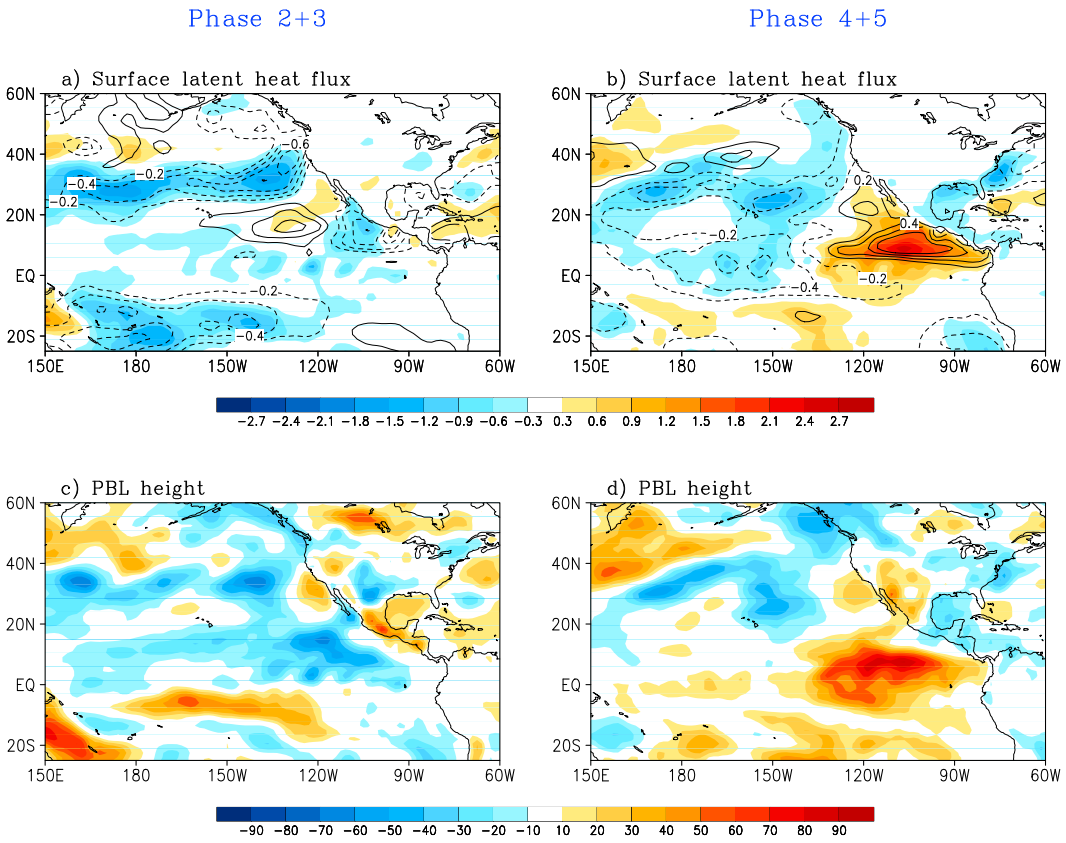

FIG. 6. Composite anomalous fields of (a),(b) upward surface latent heat flux (W m^2, shading) and 10-m wind speed (m s^{-1}, contours) and (c),(d) boundary layer height (m) during TISV phases (left) 2 + 3 and (right) 4 + 5.

Despite the observation that correlations between LTS and LCF are generally not significant as previously mentioned, composite anomalous patterns for LTS during TISV phases 2 + 3 and 4 + 5 are also examined. Results further suggest that the amplitudes in LTS anomalies are generally weak over the subtropical North Pacific; additionally, anomalous LTS patterns are also not in good agreement with the anomalous LCF patterns during these two TISV phases (not shown).

To further examine physical processes underlying the anomalous LCF patterns during different TISV phases, Figs. 6a and 6b illustrate composite surface latent heat flux (shaded) and wind speed (contours) anomalies during TISV phases 2 + 3 and 4 + 5, respectively. Reduced upward latent heat flux anomalies (shaded in blue) over the subtropical North Pacific are found to be closely collocated with the warm T-advection patterns during both TISV phases 2 + 3 and 4 + 5 (cf. Figs. 5c,d and 6a,b) and are in close agreement with anomalous LCF patterns during these two TISV phases (Figs. 3a,b). In addition to warm T advection, reduced latent heat flux anomalies are also greatly consistent with anomalous patterns of reduced total wind speed during both TISV phases (Figs. 6a,b). As northeasterly trade winds prevail over the North Pacific during summer (Fig. 1b), westerly or southwesterly winds within the 20°–40°N belt associated with anomalous cyclonic circulation during TISV phases 2 + 3 and 4 + 5 tend to weaken total trade wind speeds.

Composite anomalous patterns of PBL height based on ECMWF assimilation model output during these two TISV phases are further displayed in Figs. 6c and 6d. While the capability of the ECMWF model to capture the climatology of PBL height needs to be validated and the definition of the PBL height could be ambiguous particularly in unstable regions, we will limit our discussions of composite PBL height anomalies during different TISV phases and over regions with a well-defined marine low cloud regime. An interesting note is the remarkable association between anomalous patterns of negative PBL height and reduced surface latent heat flux over the subtropical North Pacific during both TISV phases. In particular, the comma-shaped anomalous patterns are clearly evident in both anomalous fields of surface latent heat flux and PBL height during TISV phase 4 + 5, greatly resembling the reduced LCF pattern as shown in

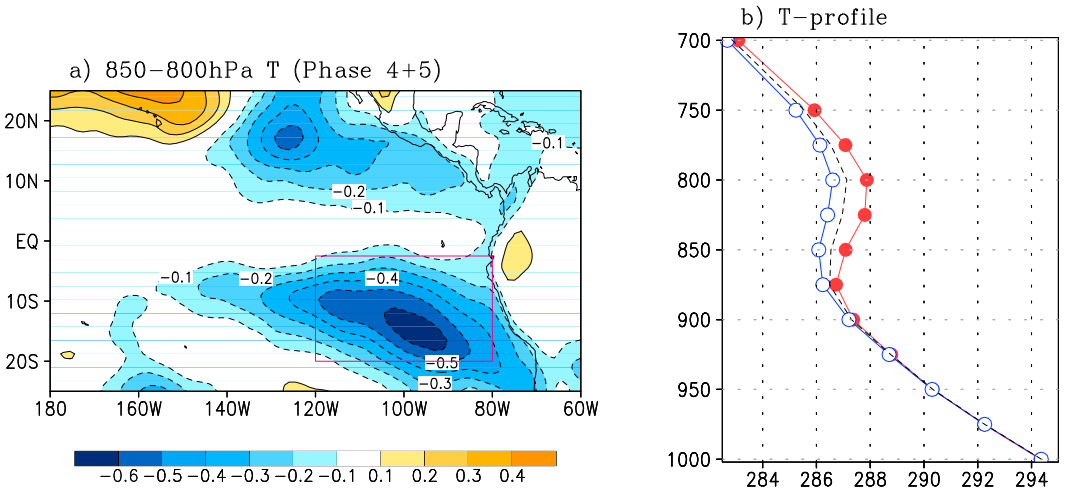

FIG. 7. (a) Composite 850–800-hPa averaged temperature anomalies (K) during eastern Pacific TISV phase 4 + 5. (b) Vertical temperature profiles (K) over the southeastern Pacific (5°–20°S, 80°–120°W); red rectangular region in (a) for climatological mean (black dashed) and TISV phases 4 + 5 (blue) and 1 + 8 (red).

Fig. 3b. In light of the complete independence between the MODIS and ECMWF datasets, this great resemblance between the anomalous LCF and surface latent heat flux as well as PBL height suggests that intraseasonal variations in PBL mixing induced by the anomalous circulation associated with the TISV could play a critical role in modulating the LCF over the subtropical North Pacific.

Next, we further explore how LCF variability over the SEPAC cold tongue region is modulated by the EPAC TISV. As shown in Fig. 4c, the strongest correlation against the intraseasonal variability of LCF over the SEPAC is found in the 800–850-hPa anomalous temperature field. The composite 850–800-hPa anomalous T pattern during TISV phase 4 + 5 is illustrated in Fig. 7a. A large area of negative temperature anomalies is present over the SEPAC, which is very consistent with the reduced local LCF pattern during this period (Fig. 3b). Note that a similar anomalous T pattern but with an opposite sign is also seen during TISV phases 1 + 8 (not shown), in agreement with enhanced LCF over the SEPAC during this period.

To further demonstrate why LCF over the SEPAC is closely related to local 850–800-hPa T anomalies, Fig. 7b displays vertical temperature profiles over the SEPAC (averaged over the purple box in Fig. 7a) for the climatological boreal summer mean (black dashed line) and composites during TISV phases 4 + 5 (blue) and 1 + 8 (red). A temperature inversion layer is readily discerned in these vertical temperature profiles, with the top of the inversion layer located near 800 hPa. Colder (warmer) than normal temperatures between 850 and 800 hPa during TISV phases 4 + 5 (1 + 8) are noted in the SEPAC as shown in Fig. 7a. As a result, the vertical temperature inversion tends to be weakened (strengthened), which give rises to a strong reduction (increase) of LCF over the SEPAC during phases 4 + 5 (1 + 8). It is worth noting that the temperature anomalies over the SEPAC associated with the EPAC TISV largely appear between 900 and 750 hPa (Fig. 7b), while anomalies over 700 and 1000 hPa are rather weak. This result is in agreement with weak intraseasonal correlations between LCF and LTS as previously mentioned, as the potential temperature differences between 1000 and 700 hPa cannot capture the changes in stability associated with this process. A modification of vertical levels for the LTS calculation is needed to accurately capture the atmospheric stability variations near the PBL inversion over this area.

Finally, by focusing on the coastal region off California, where the maximum summer mean LCF and its strongest intraseasonal variability are observed (Fig. 1), we further examine how the intraseasonal variability in LCF can influence surface radiation fluxes as well as vertical radiative (Q_R) and latent heating (LH) structures associated with the variability of LCF. Figure 8a illustrates the evolution of composite LCF (black), surface net downward SW radiation (blue), and surface upward LW radiation (green), as well as TRMM rainfall (red) anomalies over the EPAC off the Californian coast (20°–40°N, 140°–120°W; see blue box in Fig. 1a) during an EPAC TISV cycle. Consistent with results previously discussed in Fig. 3, the minimum anomalous LCF appears during TISV phases 2 and 3, and attains a maximum during TISV phase 7. Consistent with LCF, positive anomalies in downward SW radiation are evident during

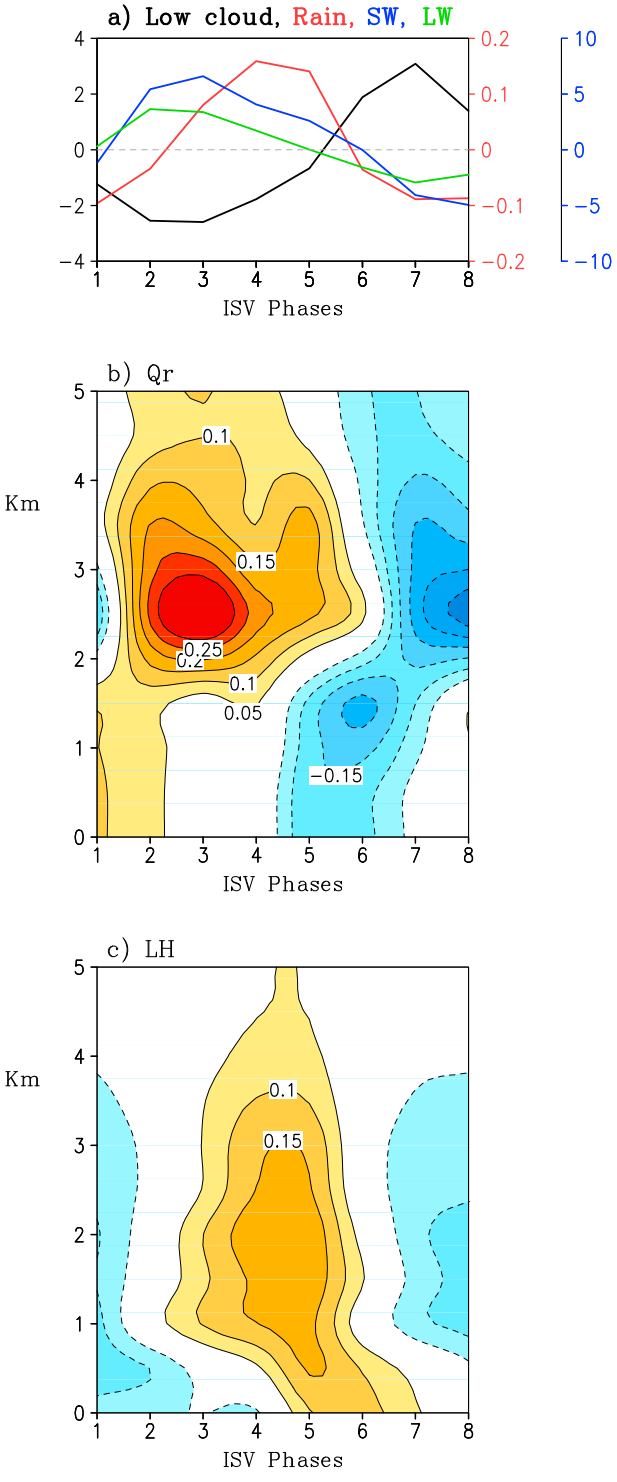

FIG. 8. (a) Evolution of low-cloud fraction (%, black curve with left y axis), rainfall (mm day^{-1}, red curve with right y axis in red), surface net downward shortwave (blue curve), and upward longwave (green curve) radiation (W m^{-2}, right y axis in blue) over the maximum summer low cloud fraction region off the California coast (15°–40°N, 145°–120°W; see blue box in Fig. 1a). Vertical profiles of (b) radiative and (c) latent heating profiles (K day^{-1}) associated with the intraseasonal low-cloud fraction variability over the same region.

TISV phases 2 and 3, while negative SW anomalies appear during TISV phases 7 and 8. The amplitude of intraseasonal variability in surface SW radiation is about 10 W m^{-2}. A generally similar evolution is seen in surface upward LW radiation anomalies. Note that the intraseasonal variability signal is also evident in the TRMM rainfall over this region although the amplitude is relatively weak. Maximum rain occurs during phases 4 and 5, following the local minimum LCF anomalies by about two phases.

Associated with reduced LCF, enhanced Q_R is observed during TISV phases 2 and 3 with a maximum being located between 2 and 3 km (Fig. 8b), largely due to reduced LW radiative cooling above cloud top. Similarly, negative Q_R is evident during TISV phases 7 and 8 in association with enhanced LCF. Corresponding to the evolution of rainfall anomalies in Fig. 8a, profiles of LH anomalies in the lower troposphere are illustrated in Fig. 8c, with positive (negative) LH anomalies during TISV phases 4 and 5 (8 and 1). Also note that the amplitude of TISV in Q_R is much stronger than that in LH (0.25 vs 0.15 K day^{-1}); particularly, during the TISV period when the maximum and minimum LCFs are observed, the amplitude of anomalous Q_R dominates that of LH. It is also noteworthy that shallow cumulus clouds associated with enhanced rainfall during the TISV phases 4 and 5 may also contribute to enhanced Q_R anomalies during this period by absorbing solar radiation in the upper portion of clouds, as noted by Ma and Kuang (2011) for clouds associated with equatorial Kelvin waves.

However, note that the composite vertical LH structure over the low cloud region off the Californian coast during TISV evolution, as illustrated in Fig. 8c, was not subject to low-cloud filtering based on the MODIS data. Therefore, the LH profile shown in Fig. 8c may partially reflect effects from some deeper precipitating congestus clouds. As suggested by Johnson and Lin (1997) based on Tropical Ocean and Global Atmosphere Coupled Ocean–Atmosphere Response Experiment (TOGA COARE) observations, LH profiles associated with trade wind cumuli over the western Pacific tend to be confined below 2.5 km. Also, caution needs to be exercised regarding uncertainties involved with the TRMM-based radiative and latent heating estimates. Very light rain from low clouds could be largely underestimated due to reported TRMM deficiencies in detecting light rain and/or small, isolated rain events (e.g., Short and Nakamura 2000; Berg et al. 2010; Jiang et al. 2011). Heating associated with nonprecipitating low clouds could also be missed in TRMM-based estimates. Additionally, the retrieval algorithms for both radiative and latent heating estimates heavily depend on lookup tables generated by cloud-resolving

models, which are further subject to parameterizations of microphysical processes.

4. Summary

Occupying a large portion of global ocean, marine low-topped clouds exert profound influences on the global energy balance. Deficiencies in representing low clouds in current GCMs thus represent a significant source of uncertainty in future climate projection. In recent decades, significant effort has been expended to achieve improved understanding of factors regulating the spatial distribution, optical properties, and temporal variability of low clouds based on observational datasets. For the variability of low clouds, previous studies have been largely focused on synoptic, annual cycle, or interannual time scales. Documentation of low cloud variability on intraseasonal time scales is rather limited. In the present study, an attempt is made to characterize low cloud variability on intraseasonal time scales, with a particular focus on the Pacific basin during boreal summer and its association with the tropical intraseasonal variability (TISV) over the EPAC ITCZ.

Widespread intraseasonal variability signals in marine low clouds during boreal summer are evident over the subtropical and midlatitude Pacific in both hemispheres, with the strongest variability found over the coastal region off California. Composite analyses of anomalous LCF patterns during different phases of the EPAC TISV suggest that the EPAC TISV may exert pronounced influences on marine low clouds over the Pacific basin. When the TISV convection is enhanced over the elongated EPAC ITCZ (TISV phase 2 + 3), reduction of LCF is detected over a vast area of the central North Pacific; meanwhile, enhanced LCFs are observed near narrow coastal regions off the North American continent extending from California to the Gulf of Alaska. In the ensuing TISV phase (phase 4 + 5), when enhanced TISV convection shifts to the northern part of the EPAC warm pool, enhancement of LCF is evident near the Hawaiian Islands and south of the Kamchatka Peninsula, while a comma-shaped negative LCF anomaly pattern extends from the subtropical North Pacific to the Gulf of Alaska. At the same time, a pronounced reduction in LCF is detected over the SEPAC during this period. Further analyses indicate that surface latent heat fluxes and PBL heights induced by anomalous low-level circulation through temperature advection and changes of total wind speed, as well as midlevel vertical velocity associated with the EPAC TISV, are the most prominent factors in regulating the intraseasonal variability of low cloud fraction over the North Pacific. For the SEPAC cold SST tongue region, temperature anomalies at the top of the boundary inversion layer between 850 and 800 hPa primarily contribute to the variability in low clouds. Results presented in this study not only provide improved understanding of low-frequency variability of marine low clouds and the underlying physics, they also provide a prominent benchmark in constraining and evaluating the representation of marine low clouds and associated coupled processes in current GCMs. Moreover, the strong modulations of the LCF by the TISV may represent a potential predictability source for subtropical and midlatitude low clouds on subseasonal time scales.

It is noteworthy that, while the present study focuses on the association of the intraseasonal variability of convective activity over the EPAC ITCZ on low cloud variability in the Pacific basin, remote influences from convective systems over other tropical regions, such as the MJO (Matthews et al. 2004), could not be completely excluded. As discussed in section 3b, while the EPAC TISV mode could be independent from the MJO forcing from the western Pacific, a large portion of TISV events over the EPAC are phase locked to the MJO condition over the Indian Ocean and western Pacific. This makes it difficult to cleanly isolate influences from the EPAC ITCZ and MJO on the low cloud variability depicted in this study. While this represents a direction for future investigation, for example, to understand dynamical or thermodynamical factors responsible for the anomalous circulation associated with the TISV as shown in Fig. 3, the main purpose of the present analysis is to document for the first time how the TISV could exert impacts on marine low clouds and to demonstrate potential predictability for low clouds on intraseasonal time scales. Hopefully, this will also motivate more analyses and studies along this line in the climate research community for comprehensive understanding of physics in regulating intraseasonal variations of marine low clouds and extensive exploration of predictability sources for intraseasonal low cloud variability.

Acknowledgments. We thank the anonymous reviewers for their insightful comments on an earlier version of this manuscript. X.J. acknowledges support by the NOAA MAPP Program under Awards NA12OAR4310075, and the NSF Climate and Large-Scale Dynamics Program under Award AGS-1228302. W.O. and X.J. acknowledge support from the NASA NEWS Program under Award NNX13AC40G. Part of this research was carried out at the Jet Propulsion Laboratory, California Institute of Technology, under a contract with the National Aeronautics and Space Administration. ISCCP surface heat flux data were provided by the WHOI OAFlux project (http://oaflux.whoi.edu).

REFERENCES

Berg, W., T. S. L'Ecuyer, and J. M. Haynes, 2010: The distribution of rainfall over oceans from spaceborne radars. *J. Appl. Meteor. Climatol.,* **49,** 535–543, doi:10.1175/2009JAMC2330.1.

Bony, S., and J.-L. Dufresne, 2005: Marine boundary layer clouds at the heart of tropical cloud feedback uncertainties in climate models. *Geophys. Res. Lett.,* **32,** L20806, doi:10.1029/2005GL023851.

Bretherton, C. S., E. Klinker, A. K. Betts, and J. A. Coakley Jr., 1995: Comparison of ceilometer, satellite, and synoptic measurements of boundary-layer cloudiness and the ECMWF diagnostic cloud parameterization scheme during ASTEX. *J. Atmos. Sci.,* **52,** 2736–2751, doi:10.1175/1520-0469(1995)052<2736:COCSAS>2.0.CO;2.

Cess, R. D., and Coauthors, 1990: Intercomparison and interpretation of climate feedback processes in 19 atmospheric general circulation models. *J. Geophys. Res.,* **95,** 16 601–16 615, doi:10.1029/JD095iD10p16601.

Dee, D. P., and Coauthors, 2011: The ERA-Interim reanalysis: Configuration and performance of the data assimilation system. *Quart. J. Roy. Meteor. Soc.,* **137,** 553–597, doi:10.1002/qj.828.

Ferranti, L., T. N. Palmer, F. Molteni, and E. Klinker, 1990: Tropical–extratropical interaction associated with the 30–60 day oscillation and its impact on medium and extended range prediction. *J. Atmos. Sci.,* **47,** 2177–2199, doi:10.1175/1520-0469(1990)047<2177:TEIAWT>2.0.CO;2.

Grecu, M., W. S. Olson, C.-L. Shie, T. S. L'Ecuyer, and W.-K. Tao, 2009: Combining satellite microwave radiometer and radar observations to estimate atmospheric heating profiles. *J. Climate,* **22,** 6356–6376, doi:10.1175/2009JCLI3020.1.

Hartmann, D. L., M. E. Ockert-Bell, and M. L. Michelsen, 1992: The effect of cloud type on Earth's energy balance: Global analysis. *J. Climate,* **5,** 1281–1304, doi:10.1175/1520-0442(1992)005<1281:TEOCTO>2.0.CO;2.

Higgins, R. W., and K. C. Mo, 1997: Persistent North Pacific circulation anomalies and the tropical intraseasonal oscillation. *J. Climate,* **10,** 223–244, doi:10.1175/1520-0442(1997)010<0223:PNPCAA>2.0.CO;2.

Hubanks, P. A., M. D. King, S. Platnick, and R. A. Pincus, 2008: MODIS atmosphere L3 gridded product. MODIS Algorithm Theoretical Basis Doc. ATBD-MOD-30, 96 pp.

Huffman, G. J., R. F. Adler, B. Rudolf, U. Schneider, and P. R. Keehn, 1995: Global precipitation estimates based on a technique for combining satellite-based estimates, rain gauge analysis, and NWP model precipitation information. *J. Climate,* **8,** 1284–1295, doi:10.1175/1520-0442(1995)008<1284:GPEBOA>2.0.CO;2.

Jiang, X., and N.-C. Lau, 2008: Intraseasonal teleconnection between North American and western North Pacific monsoons with 20-day time scale. *J. Climate,* **21,** 2664–2679, doi:10.1175/2007JCLI2024.1.

——, and D. E. Waliser, 2008: Northward propagation of the subseasonal variability over the eastern Pacific warm pool. *Geophys. Res. Lett.,* **35,** L09814, doi:10.1029/2008GL033723.

——, and ——, 2009: Two dominant subseasonal variability modes of the eastern Pacific ITCZ. *Geophys. Res. Lett.,* **36,** L04704, doi:10.1029/2008GL036820.

——, T. Li, and B. Wang, 2004: Structures and mechanisms of the northward propagating boreal summer intraseasonal oscillation. *J. Climate,* **17,** 1022–1039, doi:10.1175/1520-0442(2004)017<1022:SAMOTN>2.0.CO;2.

——, and Coauthors, 2009: Vertical heating structures associated with the MJO as characterized by TRMM estimates, ECMWF reanalyses, and forecasts: A case study during 1998/99 winter. *J. Climate,* **22,** 6001–6020, doi:10.1175/2009JCLI3048.1.

——, and Coauthors, 2011: Vertical diabatic heating structure of the MJO: Intercomparison between recent reanalyses and TRMM estimates. *Mon. Wea. Rev.,* **139,** 3208–3223, doi:10.1175/2011MWR3636.1.

——, M. Zhao, and D. E. Waliser, 2012a: Modulation of tropical cyclones over the eastern Pacific by the intraseasonal variability simulated in an AGCM. *J. Climate,* **25,** 6524–6538, doi:10.1175/JCLI-D-11-00531.1.

——, and Coauthors, 2012b: Simulation of the intraseasonal variability over the eastern Pacific ITCZ in climate models. *Climate Dyn.,* **39,** 617–636, doi:10.1007/s00382-011-1098-x.

——, E. D. Maloney, J.-L. F. Li, and D. E. Waliser, 2013: Simulations of the eastern North Pacific intraseasonal variability in CMIP5 GCMs. *J. Climate,* **26,** 3489–3510, doi:10.1175/JCLI-D-12-00526.1.

Johnson, R. H., and X. Lin, 1997: Episodic trade wind regimes over the western Pacific warm pool. *J. Atmos. Sci.,* **54,** 2020–2034, doi:10.1175/1520-0469(1997)054<2020:ETWROT>2.0.CO;2.

Klein, S. A., 1997: Synoptic variability of low-cloud properties and meteorological parameters in the subtropical trade wind boundary layer. *J. Climate,* **10,** 2018–2039, doi:10.1175/1520-0442(1997)010<2018:SVOLCP>2.0.CO;2.

——, and D. L. Hartmann, 1993: The seasonal cycle of low stratiform clouds. *J. Climate,* **6,** 1587–1606, doi:10.1175/1520-0442(1993)006<1587:TSCOLS>2.0.CO;2.

——, ——, and J. R. Norris, 1995: On the relationships among low-cloud structure, sea surface temperature, and atmospheric circulation in the summertime northeast Pacific. *J. Climate,* **8,** 1140–1155, doi:10.1175/1520-0442(1995)008<1140:OTRALC>2.0.CO;2.

Knutson, T. R., and K. M. Weickmann, 1987: 30–60 day atmospheric oscillations: Composite life cycles of convection and circulation anomalies. *Mon. Wea. Rev.,* **115,** 1407–1436, doi:10.1175/1520-0493(1987)115<1407:DAOCLC>2.0.CO;2.

Kubar, T. L., D. E. Waliser, and J.-L. Li, 2011: Boundary layer and cloud structure controls on tropical low cloud cover using A-Train satellite data and ECMWF analyses. *J. Climate,* **24,** 194–215, doi:10.1175/2010JCLI3702.1.

——, ——, ——, and X. Jiang, 2012: On the annual cycle, variability, and correlations of oceanic low-topped clouds with large-scale circulation using *Aqua* MODIS and ERA-Interim. *J. Climate,* **25,** 6152–6174, doi:10.1175/JCLI-D-11-00478.1.

Lau, W. K.-M., and D. E. Waliser, 2012: *Intraseasonal Variability in the Atmosphere–Ocean Climate System.* 2nd ed. Springer, 613 pp.

L'Ecuyer, T. S., and G. McGarragh, 2010: A 10-year climatology of tropical radiative heating and its vertical structure from TRMM observations. *J. Climate,* **23,** 519–541, doi:10.1175/2009JCLI3018.1.

Ma, D., and Z. Kuang, 2011: Modulation of radiative heating by the Madden–Julian oscillation and convectively coupled Kelvin waves as observed by CloudSat. *Geophys. Res. Lett.,* **38,** L21813, doi:10.1029/2011GL049734.

Maloney, E. D., and S. K. Esbensen, 2003: The amplification of east Pacific Madden–Julian oscillation convection and wind anomalies during June–November. *J. Climate,* **16,** 3482–3497, doi:10.1175/1520-0442(2003)016<3482:TAOEPM>2.0.CO;2.

——, and ——, 2007: Satellite and buoy observations of boreal summer intraseasonal variability in the tropical northeast Pacific. *Mon. Wea. Rev.,* **135,** 3–19, doi:10.1175/MWR3271.1.

——, D. B. Chelton, and S. K. Esbensen, 2008: Subseasonal SST variability in the tropical eastern North Pacific during boreal summer. *J. Climate,* **21,** 4149–4167, doi:10.1175/2007JCLI1856.1.

Matthews, A. J., B. J. Hoskins, and M. Masutani, 2004: The global response to tropical heating in the Madden–Julian oscillation during the northern winter. *Quart. J. Roy. Meteor. Soc.,* **130,** 1991–2011, doi:10.1256/qj.02.123.

Norris, J. R., and S. A. Klein, 2000: Low cloud type over the ocean from surface observations. Part III: Relationship to vertical motion and the regional surface synoptic environment. *J. Climate,* **13,** 245–256, doi:10.1175/1520-0442(2000)013<0245:LCTOTO>2.0.CO;2.

Randall, D. A., 1984: Stratocumulus cloud deepening through entrainment. *Tellus,* **36A,** 446–457, doi: 10.1111/j.1600-0870.1984.tb00261.x.

Reynolds, R. W., T. M. Smith, C. Liu, D. B. Chelton, K. S. Casey, and M. G. Schlax, 2007: Daily high-resolution-blended analyses for sea surface temperature. *J. Climate,* **20,** 5473–5496, doi:10.1175/2007JCLI1824.1.

Ronca, R. E., and D. S. Battisti, 1997: Anomalous sea surface temperatures and local air–sea energy exchange on intra-annual timescales in the northeastern subtropical Pacific. *J. Climate,* **10,** 102–117, doi:10.1175/1520-0442(1997)010<0102:ASSTAL>2.0.CO;2.

Rozendaal, M. A., C. B. Leovy, and S. A. Klein, 1995: An observational study of diurnal variations of marine stratiform cloud. *J. Climate,* **8,** 1795–1809, doi:10.1175/1520-0442(1995)008<1795:AOSODV>2.0.CO;2.

Rydbeck, A. V., E. D. Maloney, S.-P. Xie, J. Hafner, and J. Shaman, 2013: Remote forcing versus local feedback of east Pacific intraseasonal variability during boreal summer. *J. Climate,* **26,** 3575–3596, doi:10.1175/JCLI-D-12-00499.1.

Short, D. A., and K. Nakamura, 2000: TRMM radar observations of shallow precipitation over the tropical oceans. *J. Climate,* **13,** 4107–4124, doi:10.1175/1520-0442(2000)013<4107:TROOSP>2.0.CO;2.

Slingo, A., 1990: Sensitivity of the Earth's radiation budget to changes in low clouds. *Nature,* **343,** 49–51, doi:10.1038/343049a0.

Small, R. J., S.-P. Xie, E. D. Maloney, S. P. de Szoeke, and T. Miyama, 2011: Intraseasonal variability in the far-east Pacific: Investigation of the role of air–sea coupling in a regional coupled model. *Climate Dyn.,* **36,** 867–890, doi:10.1007/s00382-010-0786-2.

Stephens, G. L., and T. J. Greenwald, 1991: The Earth's radiation budget and its relation to atmospheric hydrology: 2. Observations of cloud effects. *J. Geophys. Res.,* **96,** 15 325–15 340, doi:10.1029/91JD00972.

Stevens, B., A. Beljaars, S. Bordoni, C. Holloway, M. Köhler, S. Krueger, V. Savic-Jovcic, and Y. Zhang, 2007: On the structure of the lower troposphere in the summertime stratocumulus regime of the northeast Pacific. *Mon. Wea. Rev.,* **135,** 985–1005, doi:10.1175/MWR3427.1.

Weare, B. C., and J. S. Nasstrom, 1982: Examples of extended empirical orthogonal function analyses. *Mon. Wea. Rev.,* **110,** 481–485, doi:10.1175/1520-0493(1982)110<0481:EOEEOF>2.0.CO;2.

Wen, M., S. Yang, W. Higgins, and R. Zhang, 2011: Characteristics of the dominant modes of atmospheric quasi-biweekly oscillation over tropical–subtropical Americas. *J. Climate,* **24,** 3956–3970, doi:10.1175/2011JCLI3916.1.

Wheeler, M. C., and H. H. Hendon, 2004: An all-season real-time multivariate MJO index: Development of an index for monitoring and prediction. *Mon. Wea. Rev.,* **132,** 1917–1932, doi:10.1175/1520-0493(2004)132<1917:AARMMI>2.0.CO;2.

Wood, R., 2012: Stratocumulus clouds. *Mon. Wea. Rev.,* **140,** 2373–2423, doi:10.1175/MWR-D-11-00121.1.

——, and C. S. Bretherton, 2006: On the relationship between stratiform low cloud cover and lower-tropospheric stability. *J. Climate,* **19,** 6425–6432, doi:10.1175/JCLI3988.1.

Zhang, Y., W. B. Rossow, A. A. Lacis, V. Oinas, and M. I. Mishchenko, 2004: Calculation of radiative fluxes from the surface to top of atmosphere based on ISCCP and other global data sets: Refinements of the radiative transfer model and the input data. *J. Geophys. Res.,* **109,** D19105, doi:10.1029/2003JD004457.

Zuidema, P., D. Painemal, S. de Szoeke, and C. Fairall, 2009: Stratocumulus cloud-top height estimates and their climatic implications. *J. Climate,* **22,** 4652–4666, doi:10.1175/2009JCLI2708.1.